RRT*-APF Hybrid Path Planning for Reconfigurable Cable-Driven Parallel Robots

Xudong Chang
College of Information and Control Engineering
Jilin Institute of Chemical Technology
Jilin, China
changxudong1@jlict.edu.cn

Ting Liu*
College of Aerospace Engineering
Jilin Institute of Chemical Technology
Jilin, China
liuting@jlict.edu.cn

Sen Jiao
College of Information and Control Engineering
Jilin Institute of Chemical Technology
Jilin, China
jiaosen@jlict.edu.cn

Zonghui Yang
College of Information and Control Engineering
Jilin Institute of Chemical Technology
Jilin, China
yangzonghui@jlict.edu.cn

2024 9th International Conference on Automation, Control and Robotics Engineering (CACRE) | 979-8-3503-5030-2/24/$31.00 ©2024 IEEE | DOI: 10.1109/CACRE62362.2024.10635035

Abstract—**When Cable-Driven Parallel Robots (CDPRs) are doing some complex work, obstacles in the environment will interfere with cables and the mobile platform. It is a meaningful work to avoid these disturbances by planning the path of CDPRs. This paper presents an optimal path planning strategy for a reconfigurable CDPR. By a variant of Rapid-exploration Random Tree (RRT) to find the optimal collision avoidance path gradually, Artificial Potential Field (APF) is used to guide the generation of random tree nodes, reducing the time of finding the path, and ensuring the safe distance between the platform and obstacles, and generating the shortest collision-free path. Post-processing algorithm reduce the number of path points. Detect whether the generated path will cause obstacles to interfere with the cable. If there is interference, optimize the robot's stiffness and minimize cable tensions to determine the optimal configuration. By adjusting the location of the cable connection points on the fixed frame, the obstacle avoidance of the cable is realized. The simulation results demonstrate the RRT*-APF hybrid path planning algorithm's ability to successfully find the path to avoid collision of the mobile platform in the environment with obstacles, the reconstruction algorithm can find the best collision-free configuration of the cable.**

Keywords—Reconfigurable cable-driven parallel robot, RRT*, APF, Path planning, Obstacle avoidance

I. Introduction

Cable-driven parallel robots (CDPRs) are mainly composed of a fixed frame and an end-effector, end-effector is driven by cables connected to the fixed frame. CDPRs are widely used in tracking camera systems[1], wind tunnel experiments[2] and astronomical observation[3-4] due to their unique advantages of lightweight design, large working space and high carrying capacity.

However, because the mobile platform is driven by multiple cables, obstacles in the working environment will interfere with the mobile platform and cables when the mobile platform is moving. Therefore, it is valuable to investigate methods for avoiding collisions with obstacles either by planning the mobile platform's path or adjusting the robot's configuration.

LaValle et al. proposed the rapid-exploration random tree (RRT) algorithm commonly used in robot path planning in 1998. The RRT algorithm quickly constructs a tree structure in free space through random sampling and rapid exploration of the environment to generate feasible paths[5]. Lahouar et al. introduced an algorithm for grid-based CDPR path planning, which is divided into two cases: the first case is that when the robot is not within the interference of obstacles, the robot moves directly towards the target point.; the second case is that when the robot enters the vicinity of the obstacle, the robot will find the best path without the interference of the obstacle. But this method decreases the variety of potential paths[6]. Bak et al. introduced an improved RRT algorithm to find paths devoid of collisions for CDPRs, using the target deviation sampling algorithm to reduce the computational load and process the resulting path to get a shorter path[7]. In order to improve the efficiency of RRT algorithm, the RRT* algorithm is proposed. In the process of path optimization, by considering the connection of a new node to the parent node of the tree and checking whether there is a shorter path that can connect the two nodes, a better path is obtained, which enables the RRT* algorithm to handle challenging path planning issues with more robustness and efficiency[8]. J. Xu et al. proposed an adaptive RRT* method, which can effectively guide tree growth through adaptive adjustment of sampling space and generate collision-free paths in chaotic environments[9]. Mishra, U.A. et al. introduce a path planning method for CDPRs that utilizes APF-RRT* and takes motion stability into account. Firstly, the collision detection is realized by combining the RRT* algorithm with the Gilbert-Johnson-Keerthi (GJK) algorithm. Then, target bias Artificial Potential Field (APF) guidance is used to shorten the convergence time and ensure directional detection[10]. However, the above path planning methods plan paths when anchor points are fixed, these methods are very effective in avoiding the interference of obstacles to the mobile platform, but in avoiding the interference of obstacles to the cable, the above method will have certain limitations.

For traditional CDPRs, most of the interference between cables and obstacles is caused by fixed cable anchor points. Therefore, a reconfigurable CDPR with movable anchor points is developed to avoid interference between cables and obstacles by reconfiguring anchor points. Gagliardini et al. investigated the reconstruction algorithm of reconfigurable CDPR for sandblasting or spray painting in cluttered environments. Anchor points on the reconfigurable CDPR are discrete and the cable connection points must be changed manually[11]. Youssef et al. introduce a method to prevent collisions among cables while the mobile platform maintains the original moving trajectory. Using an algorithm to calculate the distance between two cables, when the two cables are in close proximity, it becomes necessary to ascertain which cable is positioned higher, increase the distance from the cable below by moving the anchor point of the cable located above up[12]. An, H. et al. studied a new kind of CDPR with 8 movable cable anchor points. Each cable anchor moves independently on the track, constantly changing the configuration of the reconfigurable CDPR to avoid obstacles and keep the mobile platform moving in its intended direction.[13]. X. Wang et al. proposed a constrained path planning method to realize reconstruction of CDPRs, in the reconstruction process, anchor points position and cable length are adjusted to avoid obstacles. The restricted configuration space is built based on the implicit representation manifold, and the loop-closure constraints are established first to realize such reconfiguration. Finally, a feasible path is found in the entire constrained configuration space by using the bidirectional rapid exploration random tree in conjunction with the designed wrench feasible detection and collision detection to ensure the forward cable tension and prevent obstacle interference[14].

For CDPRs to complete some complex tasks that need to be operated on large equipment surfaces, such as painting and aircraft maintenance, the mobile platform needs to maintain a close distance from the operation object, and it is not enough to rely solely on path planning or to avoid obstacles through reconstruction. On this basis, this paper introduces a hybrid path planning method of RRT*-APF for reconfigurable CDPRs. The interference of CDPR's mobile platform and cable mainly comes from large equipment, so large equipment is treated as obstacles in the study. Since the interference of CDPRs mainly comes from the interference of obstacles to the mobile platform and cables, two kinds of interference are solved by path planning and reconstruction respectively. RRT* algorithm and APF algorithm are mixed to ensure that the path planning of the mobile platform is within the specified safe distance intervals of the obstacle, and OpenGJK is used to detect whether the swept body of the mobile platform and cables collide with the obstacle. When the path of the mobile platform will cause interference between cables and the obstacle, but the target point must be reached because of the need to work, by moving anchor points to prevent any disturbances arising from the interaction between the cable and the surface of the equipment. We choose to minimize cable tensions while maximizing stiffness as a performance index to find the optimal reconstruction.

II. INSTITUTIONAL DESCRIPTION

A. Kinematic modeling and cable tensions calculation

The reconfigurable CDPR structure diagram designed in this paper can be seen in the Fig. 1, which primarily comprises a fixed frame, a mobile platform, motors, cables, cable anchor devices and winches. Each cable anchor device is composed of an anchor point, a sliding block, a movable base, two guide screws and guide rails. The movable base is installed on the guide rail and can be moved along the guide rail by the screw drive, and the anchor point is installed on the sliding block and the sliding block is driven by the screw to move on the movable base. Four motors are connected to the winch and control the winch's rotation to release or wind cables.

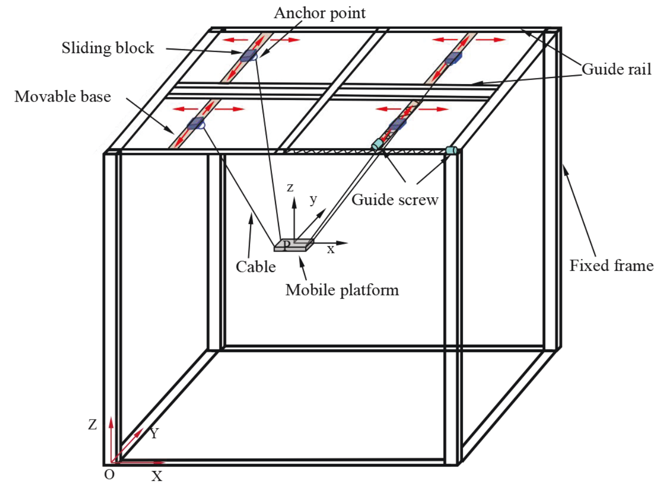

Fig. 1. Principle model of reconfigurable CDPR

In order to describe the spatial position relationship between mobile platform and fixed frame in reconfigurable cable-driven parallel robot system, the global coordinate system $O-XYZ$ and the local coordinate system $P-XYZ$, were established, as illustrated in Fig. 2.

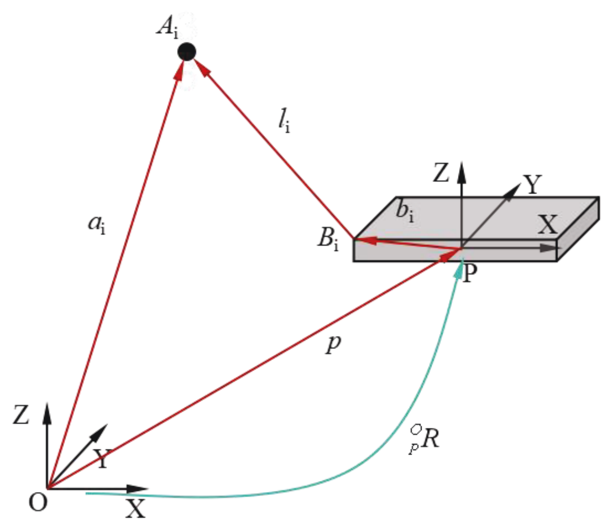

Fig. 2. Kinematics diagram of reconfigurable CDPR

$P-XYZ$ is built on the mobile platform, whereas $O-XYZ$ is built on the ground. The cable released from the winch is connected via the anchor point A_i to the connection point B_i on the mobile platform P. Each cable can be thought of as a straight line because it has much less mass than a mobile platform. The cable length l_i from A_i to B_i can be calculated by the following formula.

$$l_{\mathrm{i}}=\left\|a_{\mathrm{i}}-(p+{}_{\mathrm{P}}^{\mathrm{O}}Rb_{\mathrm{i}})\right\| \tag{1}$$

where a_{i} denotes the cable anchor point's coordinate in $O-XYZ$, p represents the coordinate of the origin of $P-XYZ$ in $O-XYZ$ and b_{i} represents the coordinate of B_{i} where the cable is connected to the mobile platform in $P-XYZ$, ${}_{P}^{O}R$ is the rotation matrix from $P-XYZ$ to $O-XYZ$, which can be expressed as

$${}_{\mathrm{P}}^{O}R=\begin{bmatrix} \mathrm{c}\beta\mathrm{c}\gamma & \mathrm{s}\alpha\mathrm{s}\beta\mathrm{c}\gamma-\mathrm{c}\alpha\mathrm{s}\gamma & \mathrm{c}\alpha\mathrm{s}\beta\mathrm{c}\gamma+\mathrm{s}\alpha\mathrm{s}\gamma \\ \mathrm{c}\beta\mathrm{s}\gamma & \mathrm{s}\alpha\mathrm{s}\beta\mathrm{s}\gamma+\mathrm{c}\alpha\mathrm{c}\gamma & \mathrm{c}\alpha\mathrm{s}\beta\mathrm{s}\gamma-\mathrm{s}\alpha\mathrm{c}\gamma \\ -\mathrm{s}\beta & \mathrm{s}\alpha\mathrm{c}\beta & \mathrm{c}\alpha\mathrm{c}\beta \end{bmatrix} \tag{2}$$

where $\mathrm{c}(\cdot)=\cos(\cdot)$, $\mathrm{s}(\cdot)=\sin(\cdot)$, and α, β, γ respectively represents the Euler Angle of rotation about the X, Y and Z axes.

The external force operating on the mobile platform and the wrench F produced by the tension of the cables have the following relationship.

$$F=JT=\begin{bmatrix} u_1 & u_2 & \dots & u_{\mathrm{n}} \\ r_1\times u_1 & r_2\times u_2 & \dots & r_{\mathrm{n}}\times u_{\mathrm{n}} \end{bmatrix}\begin{bmatrix} T_1 \; T_2 \; \cdots T_n \end{bmatrix}^{\mathrm{T}}=W_{\mathrm{e}} \tag{3}$$

where u_{n} is the vector representing each cable's length in units, the mobile platform's cable connection point's position vector is represented by r_{n}, T_{n} represents the cable tension, W_{e} represents the external force exerted on the mobile platform.

B. Stiffness matrix

The stiffness matrix K can be used to depict the mobile platform's stiffness under a single pose in its workspace. The static stiffness of the CDPR satisfies the following relation.

$$K=-\frac{\mathrm{d}J}{\mathrm{d}S}T-J\frac{\mathrm{d}T}{\mathrm{d}S}=K_1+K_2 \tag{4}$$

where $S=\left(\boldsymbol{x}^{\mathrm{T}}\ \varphi^{\mathrm{T}}\right)^{\mathrm{T}}$, $\boldsymbol{x}=(x,y,z)^{\mathrm{T}}$ is the coordinates of the point in $P-XYZ$, $\varphi=(\alpha,\beta,\gamma)^{\mathrm{T}}$ is the attitude Angle vector of the mobile platform. K_1 is the stiffness that results from the mobile platform's changing posture. K_2 is the stiffness resulting from a change in cable tensions due to a change in cable configuration.

The first term K_1 of the static stiffness matrix can be called platform pose stiffness.

$$K_1=-\frac{\mathrm{d}}{\mathrm{d}S}\begin{pmatrix} u_1 & u_2 & \dots & u_{\mathrm{n}} \\ r_1\times u_1 & r_2\times u_2 & \dots & r_{\mathrm{n}}\times u_{\mathrm{n}} \end{pmatrix}T= \sum_{i=1}^{n}\left[-\frac{\mathrm{d}}{\mathrm{d}S}\begin{pmatrix} u \\ r\times u \end{pmatrix}_{\mathrm{i}}T_{\mathrm{i}}\right] \tag{5}$$

where $-\frac{\mathrm{d}}{\mathrm{d}S}\begin{pmatrix} u \\ r\times u \end{pmatrix}_{\mathrm{i}}T_{\mathrm{i}}$ is

$$-\frac{\mathrm{d}}{\mathrm{d}S}\begin{pmatrix} u \\ r\times u \end{pmatrix}_{\mathrm{i}}T_{\mathrm{i}}=\begin{pmatrix} -\frac{\mathrm{d}u}{\mathrm{d}S} \\ -r\times\frac{\mathrm{d}u}{\mathrm{d}S}-\frac{\mathrm{d}r}{\mathrm{d}S}\times u \end{pmatrix}_{\mathrm{i}}=\begin{pmatrix} -\frac{\mathrm{d}u}{\mathrm{d}x} & -\frac{\mathrm{d}u}{\mathrm{d}\Omega} \\ -r\times\frac{\mathrm{d}u}{\mathrm{d}x}-\frac{\mathrm{d}r}{\mathrm{d}x}\times u & -r\times\frac{\mathrm{d}u}{\mathrm{d}\Omega}-\frac{\mathrm{d}r}{\mathrm{d}\Omega}\times u \end{pmatrix}_{\mathrm{i}} \tag{6}$$

where

$$-\frac{\mathrm{d}u}{\mathrm{d}\Omega}=-\left(r\times\frac{\mathrm{d}u}{\mathrm{d}x}\right)^{\mathrm{T}}=\frac{1}{l_{\mathrm{i}}}\begin{pmatrix} r_{\mathrm{z}}u_{\mathrm{x}}u_{\mathrm{y}}-r_{\mathrm{y}}u_{\mathrm{x}}u_{\mathrm{z}} & r_{\mathrm{z}}\left(1-u_{\mathrm{x}}^2\right)+r_{\mathrm{x}}u_{\mathrm{x}}u_{\mathrm{z}} & -r_{\mathrm{y}}\left(1-u_{\mathrm{x}}^2\right)-r_{\mathrm{x}}u_{\mathrm{x}}u_{\mathrm{y}} \\ -r_{\mathrm{z}}\left(1-u_{y}^2\right)-r_{\mathrm{y}}u_{\mathrm{y}}u_{\mathrm{z}} & r_{x}u_{y}u_{z}-r_{\mathrm{y}}u_{\mathrm{x}}u_{\mathrm{z}} & r_{\mathrm{x}}\left(1-u_{\mathrm{y}}^2\right)+r_{\mathrm{y}}u_{\mathrm{x}}u_{\mathrm{y}} \\ r_{\mathrm{y}}\left(1-u_{\mathrm{z}}^2\right)+r_{\mathrm{z}}u_{\mathrm{y}}u_{\mathrm{z}} & -r_{\mathrm{x}}\left(1-u_{\mathrm{z}}^2\right)-r_{\mathrm{z}}u_{\mathrm{x}}u_{\mathrm{z}} & r_{y}u_{\mathrm{x}}u_{z}-r_{x}u_{y}u_{\mathrm{z}} \end{pmatrix} \tag{6a}$$

$$-r\times\frac{\mathrm{d}u}{\mathrm{d}\Omega}=\frac{1}{l_{\mathrm{i}}}\begin{pmatrix} r_{\mathrm{y}}^2+r_{\mathrm{z}}^2-\left(r_{\mathrm{y}}u_{\mathrm{z}}-r_{\mathrm{z}}u_{\mathrm{y}}\right)^2 & -r_{\mathrm{x}}r_{\mathrm{y}}-\left(r_{\mathrm{y}}u_{\mathrm{z}}-r_{\mathrm{z}}u_{\mathrm{y}}\right)\left(r_{\mathrm{z}}u_{\mathrm{x}}-r_{\mathrm{x}}u_{\mathrm{z}}\right) & -r_{\mathrm{z}}r_{\mathrm{x}}-\left(r_{\mathrm{x}}u_{\mathrm{y}}-r_{\mathrm{y}}u_{\mathrm{x}}\right)\left(r_{\mathrm{y}}u_{\mathrm{z}}-r_{\mathrm{z}}u_{\mathrm{y}}\right) \\ & r_{\mathrm{z}}^2+r_{\mathrm{x}}^2-\left(r_{z}u_{\mathrm{x}}-r_{x}u_{\mathrm{z}}\right)^2 & -r_{z}r_{\mathrm{y}}-\left(r_{\mathrm{x}}u_{\mathrm{y}}-r_{y}u_{\mathrm{x}}\right)\left(r_{z}u_{\mathrm{x}}-r_{x}u_{\mathrm{z}}\right) \\ & & r_{\mathrm{x}}^2+r_{\mathrm{y}}^2-\left(r_{\mathrm{x}}u_{\mathrm{y}}-r_{\mathrm{y}}u_{\mathrm{x}}\right)^2 \end{pmatrix} \tag{6b}$$

$$-\frac{\mathrm{d}r}{\mathrm{d}x}\times u=\begin{pmatrix} 0 & -u_{\mathrm{z}} & u_{\mathrm{y}} \\ u_{\mathrm{z}} & 0 & -u_{\mathrm{x}} \\ -u_{\mathrm{y}} & u_{\mathrm{x}} & 0 \end{pmatrix} \tag{6c}$$

$$-\frac{\mathrm{d}r}{\mathrm{d}\Omega}\times u=\begin{pmatrix} r_{\mathrm{y}}u_{\mathrm{y}}+r_{\mathrm{z}}u_{\mathrm{z}} & -r_{\mathrm{x}}u_{\mathrm{y}} & -r_{\mathrm{x}}u_{\mathrm{z}} \\ -r_{\mathrm{y}}u_{\mathrm{x}} & r_{\mathrm{x}}u_{\mathrm{x}}+r_{\mathrm{z}}u_{\mathrm{z}} & -r_{\mathrm{y}}u_{\mathrm{z}} \\ -r_{\mathrm{z}}u_{\mathrm{x}} & -r_{\mathrm{z}}u_{\mathrm{y}} & r_{\mathrm{x}}u_{\mathrm{x}}+r_{\mathrm{y}}u_{\mathrm{y}} \end{pmatrix} \tag{6d}$$

$$-\frac{\mathrm{d}u}{\mathrm{d}x}=\frac{1}{l_{\mathrm{i}}}\begin{pmatrix} 1-u_{\mathrm{x}}^2 & -u_{\mathrm{x}}u_{\mathrm{y}} & -u_{\mathrm{x}}u_{\mathrm{z}} \\ & 1-u_{\mathrm{y}}^2 & -u_{\mathrm{y}}u_{\mathrm{z}} \\ & & 1-u_{\mathrm{z}}^2 \end{pmatrix} \tag{6e}$$

The second term K_2 of the static stiffness matrix can be called the positional stiffness of cables.

$$K_2=-J\cdot\frac{\mathrm{d}T}{\mathrm{d}x}=J\cdot\mathrm{diag}\left(\frac{E_1A_1}{l_1}\ \frac{E_2A_2}{l_2}\ \dots\ \frac{E_{\mathrm{n}}A_{\mathrm{n}}}{l_{\mathrm{n}}}\right)\cdot J^{\mathrm{T}} \tag{7}$$

A_n signifies the cable's cross-sectional area, and E_n stands for the cable's elastic modulus.

III. RRT*-APF HYBRID ALGORITHM

A. Hybrid algorithm

In this section, combined with the actual work needs of CDPRs, a hybrid RRT*-APF algorithm is proposed to determine the optimal collision-free path within the specified safe distance interval of the obstacle surface without considering the cable collision. From the starting point x_{start}, the random tree grows, and then grows in the direction of the target point, constantly generating new nodes x_{new}. The target point x_{goal} is considered reached when the new node x_{new}'s distance to the target point x_{goal} is smaller than a predetermined threshold value r_g. The algorithm creates the shortest path free of collisions and breaks the loop. In the process of generating a new node x_{new}, the hybrid artificial Potential field method (APF) is used. First, random point x_{rand} is generated in the ball with the goal point x_{goal} as the center of the sphere and r_r as the radius. Random points guided by the target point can be selected faster to find the shortest feasible path. Find the point x_{near} that is closest to the random point among all nodes in the tree. The mobile platform is subject to the attraction force of x_{rand}, the attraction force of x_{goal}, and the attraction or repulsive force of obstacles. The attraction or repulsive forces are as follows.

The attraction force exerted by random point and target point on the mobile platform remains constant, specifically,

$$\begin{cases} F_{goal} = \dfrac{\left(x_{goal} - x_{near}\right)}{\left\| x_{goal} - x_{near} \right\|} \\ F_{rand} = \dfrac{\left(x_{rand} - x_{near}\right)}{\left\| x_{rand} - x_{near} \right\|} \end{cases} \tag{8}$$

The distance from the mobile platform to the obstacle determines whether the mobile platform receives the obstacle's attraction or repulsive force, and also determines the magnitude of the force. The upper limit and lower limit of the safety distance interval can be set as x_{upper} and x_{lower} respectively according to the actual requirements, when $\frac{x_{lower} + x_{upper}}{2} < \rho\left(x_{near}, x_{obs}\right) < x_{upper}$, the mobile platform is subject to the attraction force of the obstacle, and the force's magnitude increase with increasing distance and decreases with decreasing distance; when $x_{lower} < \rho\left(x_{near}, x_{obs}\right) < \frac{x_{lower} + x_{upper}}{2}$, the mobile platform is subject to the repulsive force of the obstacle, and the force's magnitude decreases with increasing distance; conversely, the force's magnitude increases with decreasing distance. The attraction potential field function U_{att} is as follows.

$$U_{att} = \frac{1}{2}\eta\rho^2\left(x_{near}, x_{obs}\right), \frac{x_{lower} + x_{upper}}{2} < \rho\left(x_{near}, x_{obs}\right) < x_{upper} \tag{9}$$

where η is the proportional gain coefficient, $\rho\left(x_{near}, x_{obs}\right)$ as a vector, Represents the distance from the mobile platform x_{near} to the obstacle x_{obs}. The direction originates from the mobile platform and extends towards the obstacle. The attraction force F_{att} corresponding to this is derived from the negative gradient of the attraction potential field.

$$\begin{gathered} F_{att} = -\nabla U_{att}\left(x\right) = \eta\rho\left(x_{near}, x_{obs}\right), \\ \frac{x_{lower} + x_{upper}}{2} < \rho\left(x_{near}, x_{obs}\right) < x_{upper} \end{gathered} \tag{10}$$

The repulsive potential field function U_{rep} is as follows

$$\begin{gathered} U_{rep} = \frac{1}{2}k\left(\frac{1}{\rho\left(x_{obs}, x_{near}\right)} - \frac{1}{\frac{x_{lower} + x_{upper}}{2}}\right)^2, \\ x_{lower} < \rho\left(x_{obs}, x_{near}\right) < \frac{x_{lower} + x_{upper}}{2} \end{gathered} \tag{11}$$

where k is a constant and $\rho\left(x_{obs}, x_{near}\right)$ is a vector, representing the distance from the mobile platform x_{near} to the obstacle x_{obs}, the direction originates from the obstacle and extends towards the mobile platform. The repulsive force F_{rep} corresponding to this is derived from the negative gradient of the repulsive potential field.

$$F_{rep} = -\nabla U_{rep}\left(x\right) = k\left(\frac{1}{\rho\left(x_{obs}, x_{near}\right)} - \frac{1}{\frac{x_{lower} + x_{upper}}{2}}\right) \cdot \frac{1}{\rho^2\left(x_{obs}, x_{near}\right)}, x_{lower} < \rho\left(x_{obs}, x_{near}\right) < \frac{x_{lower} + x_{upper}}{2} \tag{12}$$

According to the above analysis, there are the following three situations:

(1) When the distance is greater than x_{upper}, the mobile platform is only subject to the attraction of the target point F_{goal} then the value of x_{new} is

$$x_{new} = x_{near} + v_{step} \cdot F_{goal} \tag{13}$$

where v_{step} is the step size.

(2) When the distance is greater than $\frac{x_{\text{lower}} + x_{\text{upper}}}{2}$ and less than x_{upper}, the mobile platform is subjected to the force F_{res1} of unit size in the resultant direction of the attraction force F_{goal} along the target point, the attraction force F_{rand} of random points and the attraction force F_{att} of obstacles, then the value of x_{new} is

$$x_{\text{new}} = x_{\text{near}} + v_{\text{step}} \cdot F_{res1} = x_{\text{near}} + v_{\text{step}} \cdot \frac{\left(F_{\text{goal}} + F_{\text{rand}} + F_{\text{att}}\right)}{\left\| F_{\text{goal}} + F_{\text{rand}} + F_{\text{att}} \right\|} \quad (14)$$

(3) When the distance is greater than x_{lower} and less than $\frac{x_{\text{lower}} + x_{\text{upper}}}{2}$, the mobile platform is subjected to the force F_{res2} of unit size in the resultant direction of the attraction force F_{goal} along the target point, the attraction force F_{rand} of random points and the obstacle's repulsive force F_{att}, then the value of x_{new} is

$$x_{\text{new}} = x_{\text{near}} + v_{\text{step}} \cdot F_{res2} = x_{\text{near}} + v_{\text{step}} \cdot \frac{\left(F_{\text{goal}} + F_{\text{rand}} + F_{\text{rep}}\right)}{\left\| F_{\text{goal}} + F_{\text{rand}} + F_{\text{rep}} \right\|} \quad (15)$$

In the field of x_{near}, find the node x_{best} with shorter path cost, and then replace x_{near} with x_{best} to connect with x_{new}, calculate the distance the mobile platform is from the obstacle, and determine whether it is a safe distance. If it is not, continue to find the next parent node, and if there is no parent node conforming to the safe distance, abandon x_{new} and rebuild.

B. Collision detection

This section mainly introduces the collision detection method of mobile platform. In this paper, OpenGJK fast detection algorithm[15] is adopted to detect obstacle collision, so as to achieve faster and more accurate collision detection. OpenGJK fast detection algorithm can calculate the distance between two convex polyhedra, approximate the mobile platform and obstacles as convex polyhedra, for the cylinder, can calculate the distance from the mobile platform to the obstacle and the central axis of the cylinder, minus the radius of the cylinder is the distance from the surface of the cylinder. For a mobile platform, to ensure a safe distance from the obstacle on the path from x_{start} to x_{goal}, it is necessary to determine whether the swept body of the mobile platform can maintain a safe distance from the obstacle between two nodes. The convex hull algorithm is used to determine the swept body of the mobile platform. As illustrated in Fig. 3, it is the schematic diagram of collision between the swept body of the mobile platform and the obstacle and maintaining a safe distance.

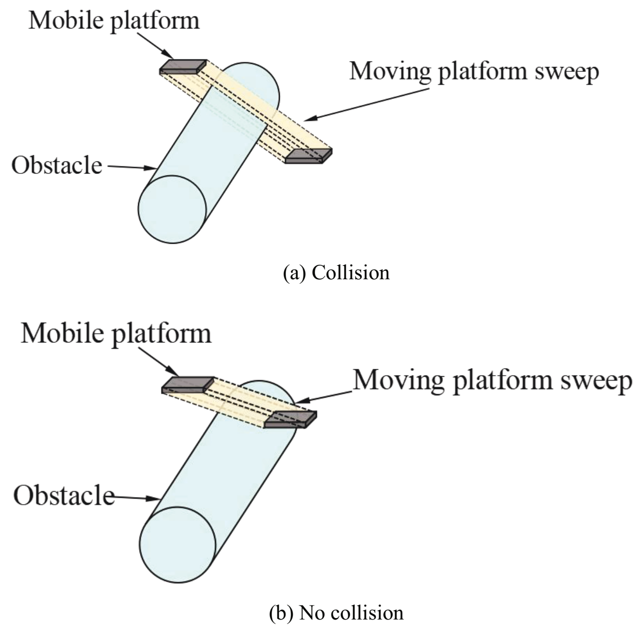

Fig. 3. Schematic diagram of collision between mobile platform and obstacle

C. Path post-processing

After the collision-free path of the mobile platform is obtained, it goes through a post-processing process. The skimmed body is generated from the initial point and subsequent path points in turn, and the safe distance between the skimmed body and the mobile platform is judged until the initial point is connected to the farthest path point conforming to the safe distance, and the middle path point is abandoned. With the farthest path point conforming to the safety distance as the initial point, repeat the above steps until the connection to the target point, and complete the post-processing of the resulting path. As illustrated in Fig. 4, this process can effectively reduce the number of path points and obtain a simpler collision-free path.

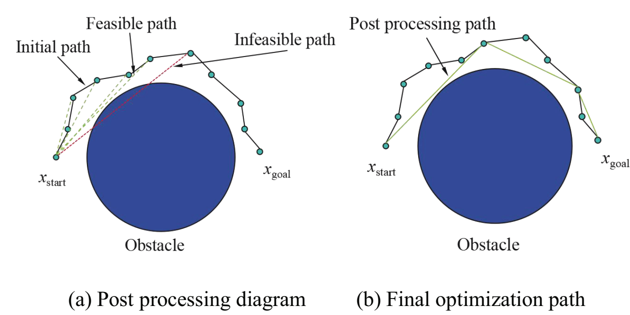

Fig. 4. Schematic diagram of path post-processing process

IV. Reconfiguration Strategy of Cable-Driven Parallel Robot

The collision-free path of the mobile platform has been obtained in the previous section. The path of the mobile platform from x_{start} to x_{goal} is discretized into n path points, expressed as

$$x = \left[x_{\text{start}}, x_1, x_2, \cdots, x_{\text{goal}}\right] \tag{16}$$

Since the cable can only be pulled and cannot be pushed, the lower limit of tension $T_{\min}$ should be greater than zero, and the upper limit of tension should be restricted by the motor's maximum torque. The working space of a CDPR is usually irregular and limited by tension boundaries. Therefore, when a mobile platform performs a task, the path may include points that are not in the workspace, and the mobile platform cannot safely reach the path point without changing the location of anchor points. Another problem is that in the process of moving the platform to some necessary positions, obstacles may interfere with the cable, causing serious consequences. Therefore, it should be ensured that the distance between the swept body of the cable and the obstacle during the movement is exceeds the minimum safe distance $D_{\min}$, and the cable anchor points' positions should be changed to avoid the interference caused by the obstacle to the cable. As illustrated in Fig. 5, the collision between the swept body of the cable and the obstacle and the safe distance are respectively schematic diagrams.

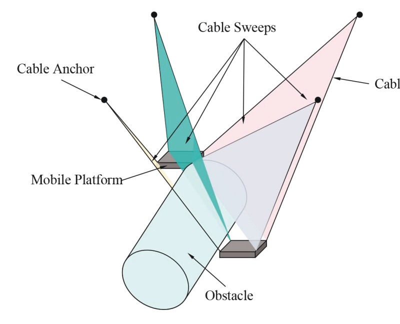

(a) Collision

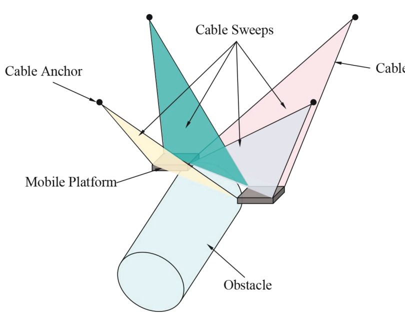

(b) No collision

Fig. 5. Schematic diagram of collision between a cable sweep and an obstacle

In this section, Particle Swarm Optimization (PSO) algorithm is used to calculate the optimal position of each anchor point in the configurable region while maintaining the collision free path of the mobile platform. To obtain a suitable refactoring solution, we consider two objectives. The first objective is to minimize the total cable tensions, as this metric is closely linked to the reconfigurable CDPR's power consumption. Maximizing the stiffness of the reconfigurable CDPR is the second objective. Therefore, the objective function is written as

$$F(T, K) = \min\left(\frac{\sum_{i=1}^{n} T_{\mathrm{i}}}{\|K\|}\right) \tag{17}$$

The constraint is set to:

$$\begin{cases} T_{\min} < T < T_{\max} \\ D_{\min} < D \\ X_{\mathrm{i}\min} < X_{\mathrm{i}} < X_{i\max} \\ Y_{i\min} < Y_i < Y_{i\max} \\ JT = W_{\mathrm{e}} \end{cases} \tag{18}$$

$T_{\min}$ and $T_{\max}$ respectively represent the cable tension's lower and upper limits. D and $D_{\min}$ are the distance and lower limit of distance of cable and obstacle respectively. X_{i}, X_{imin} and X_{imax} are the X coordinates, lower and upper limits of X coordinates of the ith anchor point in $O-XYZ$, respectively. Y_{i}, Y_{imin} and Y_{imax} are respectively the Y coordinate, lower and upper limits of Y coordinates of the ith anchor point in $O-XYZ$. The aforementioned reconstruction problems are resolved using the PSO algorithm, whose computation procedure is illustrated in Fig 6.

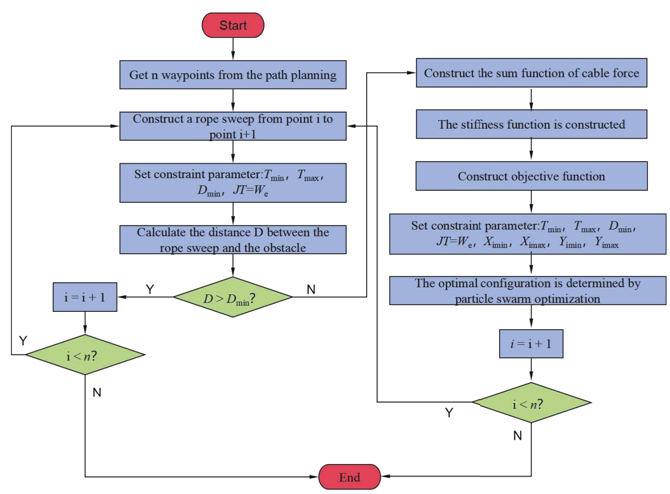

Fig. 6. Reconstruction algorithm diagram

Reconfigurable CDPR can be considered as a collection of CDPRs with different configuration of anchor points, which will increase the working space of the robot to a certain extent. The algorithm will calculate in advance whether the next path point satisfies the cable tension's upper and lower limits , and whether the distance from cables to the obstacle during the movement to the next point is greater than the specified safety distance. If both meet the requirements, the reconstruction will not be triggered. If one item does not meet the requirements, the reconstruction will be triggered, and cable anchor points will be reconfigured before the mobile platform starts to run to the next path point.

V. SIMULATION EXPERIMENT

Simulation is performed to assess the proposed path planning algorithm's performance and reconstruction method. The fixed frame of the CDPR is a cuboid frame with a size of $2m$, $1.5m$ and $1.8m$, and the mobile platform is a cube with a size of $0.2m$, $0.2m$ and $0.1m$ and a weight of $1kg$. The anchor points' original positions are set at the corners of the fixed frame, and the first anchor point's reachable position is $X_1[0,\ 0.95]$, $Y_1[0,\ 0.7]$, the second anchor point's reachable position is $X_2[1.05,\ 2]$, $Y_2[0,\ 0.7]$, the third anchor point's reachable position is $X_3[1.05,\ 2]$, $Y_3[0.8,\ 1.5]$, the fourth anchor point's reachable position is $X_4[0,\ 0.95]$, $Y_4[0.8,\ 1.5]$, The minimum and maximum permissible cable tension is established at $1N$ and $300N$,respectively.

In order to prove the proposed path planning algorithm's efficacy, the obstacle in the environment is modeled as a cylinder with a radius of $0.25m$ and a length of $1m$, with the two endpoints of the central axis of the cylinder located at $(0.5,\ 0.75,\ 0.5)$ and $(1.5,\ 0.75,\ 0.5)$, the safe distance from the mobile platform to the obstacle is set within the range of $0.01m$ to $0.02m$.

Firstly, the proposed RRT*-APF hybrid algorithm is used to obtain the desired approach optimal path from the starting point $x_{start}[1.4,\ 0.75,\ 1.32]$ to the target point $x_{goal}[1.4,\ 1.115,\ 1]$ in an environment with cylindrical obstacles. Fig. 7a and Fig. 7b show the collision-free path and the post-processed path from x_{start} to x_{goal} respectively. The post-processing algorithm successfully reduces the number of path points from 32 to 7. Fig 8a and Fig 8b respectively show the distance from the mobile platform to the obstacle in the path from x_{start} to x_{goal} before post-processing and after post-processing. The red line is the set safe distance interval. It can be seen from the figure that the mobile platform is within the safe distance interval during the whole path process.

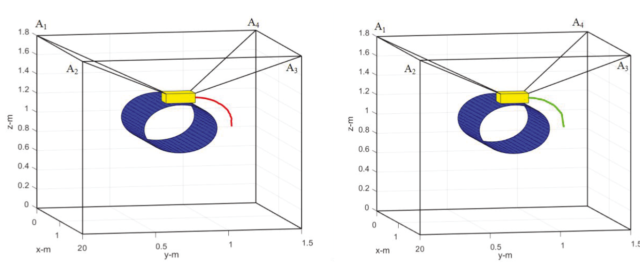

(a) Collision-free path (b) Post-processed collision free path

Fig. 7. Simulated environmental result

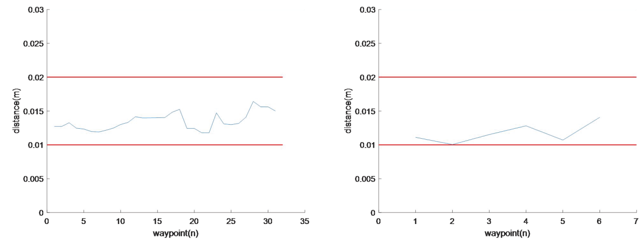

(a) (b)

Fig. 8. Distance between the mobile platform and the obstacle

Regarding cables, when the sixth path point is reached by the mobile platform, cables 1 and 2 will collide with the obstacle. Reconstruction begins when the mobile platform reaches the fifth path point. After the reconstruction of cable anchor points is completed, the mobile platform will continue to move the remaining path points until the target point is reached. Fig. 9a and Fig. 9b respectively show the positions of cord points before and after reconstruction. Fig. 10 shows the distance from the four cables to the obstacle in the path from x_{start} to x_{goal} , and the red line is the set safe distance threshold. It can be seen from the figure that the four cables are all at a safe distance during the whole path process.

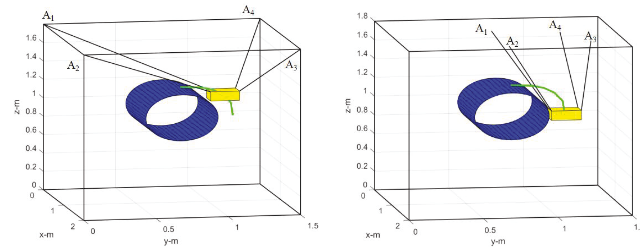

(a) Initial structure (b) Reconfigured structure

Fig. 9. Reconstruction result

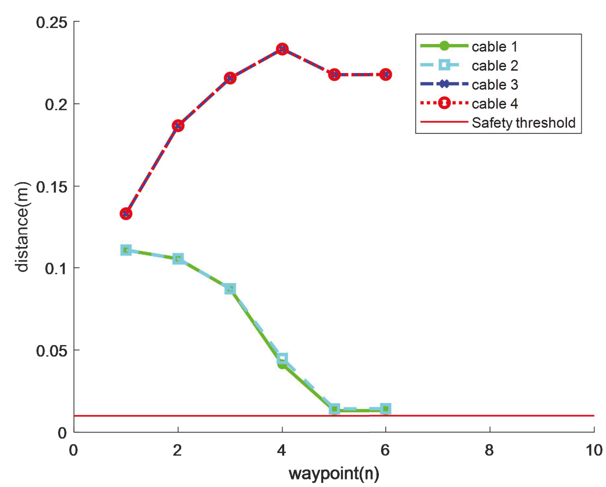

Fig. 10. Distance between cable and obstacle

VI. CONCLUSION

In this paper, a RRT*-APF hybrid path planning algorithm is proposed for reconfigurable CDPR. By guiding the generation of random tree nodes by APF, from the starting point to the destination, determine the best viable path that avoids collisions. For the path points where obstacles will interfere with cables, the optimal configuration of maximizing the robot stiffness and minimizing the sum of cable tensions is selected based on the cable tensions and distance detection. The obstacle avoidance of the cable is realized by adjusting the anchor point positions. The proposed path planning algorithm's effectiveness is confirmed through simulation experiments.

REFERENCES

[1] Tanaka M, Seguchi Y, Shimada S. Kineto-Statics of Skycam-Type Wire Transport System[C] // Proceedings of USA-Japan symposium on flexib le automation, Crossing bridges: advances in flexible automation and ro botics. 1988 : 689-694.

[2] Jensen, F.V, Kjærulff U, Kristiansen B, Langseth H, Skaanning C, Voml el J, & Vomlelov323á M. (2001). The SACSO methodology for troubles hooting complex systems. Artificial Intelligence for Engineering Design, Analysis and Manufacturing, 15, 321-333.

[3] Yao R, Tang X, Wang J, & Huang P. (2010). Dimensional Optimization Design of the Four-Cable-Driven Parallel Manipulator in FAST. IEEE/ASME Transactions on Mechatronics, 15, 932-941.

[4] Shao Z, Tang X, Chen X, Wang L. Driving force analysis for the second ary adjustable system in FAST[J]. Robotica, 2011,29(6): 903-915.

[5] LaValle SM (1998) Rapidly-exploring random trees: a new tool for path planning.

[6] Lahouar S, Ottaviano E, Zeghoul S, Romdhane L, Ceccarelli M (2009) Collision free path-planning for cable-driven parallel robots. Robot Auton Syst 57(11):1083–1093.

[7] Bak JH, Hwang SW, Yoon J, Park JH, Park JO (2019) Collision-free path planning of cable-driven parallel robots in cluttered environments. Intel Serv Robot 12(3):243–253.

[8] Karaman S, Frazzoli E (2011) Sampling-based algorithms for optimal motion planning. Int J Robot Res 30(7):846–894.

[9] Xu, J., & Park, K. (2022). Kinematic performance-based path planning for cable-driven parallel robots using modified adaptive RRT*. Microsystem Technologies, 28, 2325-2336.

[10] Mishra, U.A., Métillon, M., & Caro, S. (2021). Kinematic Stability based APF-RRT* Path Planning for Cable-Driven Parallel Robots †. 2021 IEEE International Conference on Robotics and Automation (ICRA), 6963-6969.

[11] L. Gagliardini, S. Caro, M. Gouttefarde, P. Wenger, and A. Girin, “A reconfigurable cable-driven parallel robot for sandblasting and painting of large structures,” in Cable-Driven Parallel Robots. Berlin/Heidelberg,Germany: Springer, 2015, pp. 275–291.

[12] K. Youssef and M. J.-D. Otis, “Reconfigurable fully constrained cable driven parallel mechanism for avoiding interference between cables,” Mech. Mach. Theory 148, 103781 (2020).

[13] An, H., Yuan, H., Tang, K.W., Xu, W., & Wang, X. (2022). A Novel Ca ble-Driven Parallel Robot With Movable Anchor Points Capable for Obs tacle Environments. IEEE/ASME Transactions on Mechatronics, 27, 54 72-5483.

[14] X. Wang, B. Zhang, W. Shang, F. Zhang and S. Cong, "Constrained Path Planning for Reconfiguration of Cable-Driven Parallel Robots," in IEEE/ASME Transactions on Mechatronics, vol. 28, no. 4, pp. 2352-2363, Aug. 2023.

[15] M. Montanari and N. Petrinic, “OpenGJK for C, C# and Matlab: Reliable solutions to distance queries between convex bodies in three-dimensional space,” SoftwareX, vol. 7, pp. 352–355, 2018.